

## Report

# Two Kinesins Are Involved in the Spatial Control of Cytokinesis in *Arabidopsis thaliana*

Sabine Müller,<sup>1,\*</sup> Shengcheng Han,<sup>1,2</sup> and Laurie G. Smith<sup>1</sup>

<sup>1</sup>Section of Cell and Developmental Biology  
University of California, San Diego  
La Jolla, California 92093

## Summary

In plant cells, the plane of division is anticipated at the onset of mitosis by the presence of a preprophase band (PPB) of microtubules and F-actin at a cortical site that circumscribes the nucleus. During cytokinesis, the microtubule- and F-actin-based phragmoplast facilitates construction of a new cell wall and is guided to the forecast division site. Proper execution of this process is essential for establishing the cellular framework of plant tissues. The microtubule binding protein TANGLED1 (TAN1) of maize is a key player in the determination of division planes [1–3]. Lack of TAN1 leads to misguided phragmoplasts and mispositioned cell walls in maize. In a yeast two-hybrid screen for TAN1-interacting proteins, a pair of related kinesins was identified that shares significant sequence homology with two kinesin-12 genes in *Arabidopsis thaliana* (*A. thaliana*): PHRAGMOPLAST ORIENTING KINESIN 1 and 2 (*POK1*, *POK2*). *POK1* and *POK2* are expressed in tissues enriched for dividing cells. The phenotype of *pok1;pok2* double mutants strongly resembles that of maize *tan1* mutants, characterized by misoriented mitotic cytoskeletal arrays and misplaced cell walls. We propose that *POK1* and *POK2* participate in the spatial control of cytokinesis, perhaps via an interaction with the *A. thaliana* TAN1 homolog, ATN.

## Results and Discussion

The plant cytoskeleton undergoes meticulously conducted rearrangements to establish the division plane prior to mitosis, separate chromosomes at mitosis, and form a new cell wall at cytokinesis in the previously established division plane. Throughout prophase, the future division plane is predicted by the position of the cortical preprophase band (PPB) of microtubules and actin filaments [4]. As cells enter mitosis, the PPB is disassembled while microtubules form the spindle, leaving behind an actin-depleted zone in the cell cortex, which marks the former location of the PPB throughout mitosis and cytokinesis [4]. Recent work has shown that a plasma membrane-localized *A. thaliana* kinesin, KCA1, is excluded from the PPB zone during prophase, and like cortical F-actin remains locally depleted at the former PPB site throughout the remainder of the cell cycle

[5]. After mitosis, cytoplasmic microtubules and F-actin are reorganized to form a phragmoplast, which facilitates formation of the cell plate (the new cell wall) via the fusion of Golgi-derived vesicles [6]. The phragmoplast is initiated in isolation from the parental plasma membrane and cell wall, and subsequently expands to attach the cell plate to the parental wall at the site formerly occupied by the PPB (“the division site”). It has been proposed that PPB-dependent modification(s) of the cell wall, plasma membrane, and/or cell cortex guide phragmoplast expansion toward the division site [7]. Local depletion of F-actin and KCA1 at the division site are likely to be important for phragmoplast guidance [4, 5]; both pharmacological and genetic studies suggest important roles for actin and myosin in this process [8–10]. For the most part, however, mechanisms governing phragmoplast guidance remain mysterious.

The TAN1 protein of maize plays an important role in the orientation of cell division planes and is one of the few proteins known to be involved in the spatial control of cytokinesis. TAN1 is a novel, highly basic protein that binds to microtubules in vitro and belongs to a family of proteins that are preferentially localized to mitotic microtubule arrays in dividing cells [1]. In *tan1* mutants, PPBs are occasionally misoriented and the majority of phragmoplasts fail to be guided to former PPB sites, pointing to a role for TAN1 in phragmoplast guidance [2].

A yeast two-hybrid screen for interaction partners of TAN1 led to the isolation of two truncated, predicted coiled-coil forming maize proteins, which are related to each other and to the carboxy (COOH)-terminal tails of two predicted *A. thaliana* kinesins, *POK1* (At3g17360) and *POK2* (At3g19050). One of the maize protein fragments is most similar to *POK1* (43% identical over its entire length of 435 amino acids), while the other is most similar to *POK2* (30% identical over its entire length of 439 amino acids). RT-PCR analysis revealed that *POK1* is comprised of 34 exons, encoding a protein of 2066 amino acids and a molecular weight of 234 kDa, while *POK2* is comprised of 36 exons, encoding a protein of 2770 amino acids and a predicted molecular weight of 315 kDa (Figures 1A and 1B, and Figure S2A in the Supplemental Data available with this article online). Protein-protein interaction between the C terminus of *POK1* and the *A. thaliana* TAN1 homolog, ATN (At3g05330), was confirmed in directed yeast two-hybrid experiments (Figure S1), suggesting that ATN and *POK1* could act together.

In *A. thaliana*, 61 putative kinesins have been identified based on the presence of the characteristic motor domain [11, 12]. *POK1* and *POK2* are most closely related to each other and, based on sequence homology in their motor domains, belong to the kinesin-12 class [13], which includes the well-characterized group of phragmoplast-associated kinesins AtPAKRPs [14] (Figure S2B). Both kinesins are composed of an N-terminal motor domain (Figure S2A) followed by coiled-coil domains (predicted by COILS program (<http://www.ch>

\*Correspondence: [smuller@biomail.ucsd.edu](mailto:smuller@biomail.ucsd.edu)

<sup>2</sup>Present address: Department of Biology, University of Virginia, Charlottesville, Virginia 22904.

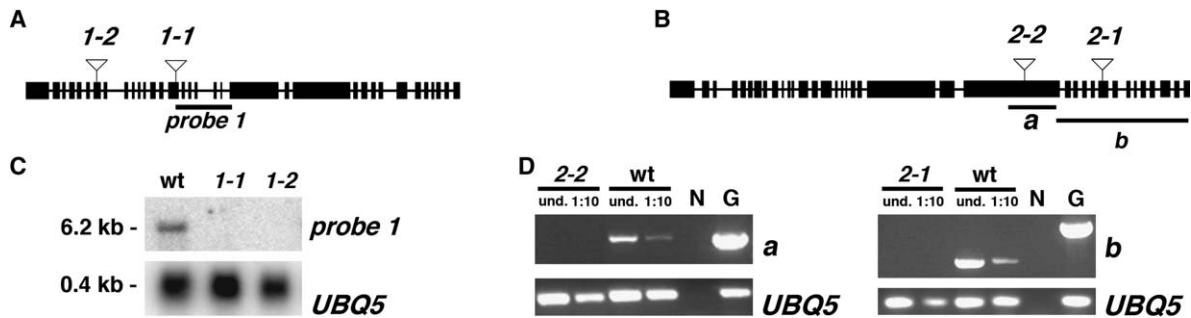


Figure 1. *POK1* and *POK2* Gene Structure and Mutations

(A) Exon/intron structure of *POK1* showing the locations of T-DNA insertions in *pok1-1* (exon 15) and *pok1-2* (exon 7) alleles.  
 (B) Exon/intron structure of *POK2* showing the locations of T-DNA insertions in *pok2-1* (exon 28) and *pok2-2* (exon 23) alleles. Exons are shown as black bars, introns are shown as lines. The complete coding sequence for each gene was determined by RT-PCR analysis, by means of primers listed in Table S2.  
 (C) Northern blot analysis of *POK1* gene expression in wild-type (Columbia), *pok1-1* and *pok1-2* mutant backgrounds. The *POK1* probe (located as illustrated in [A]) was PCR amplified with primers POK1-XbaI/NruI and POK1-SpeI (Table S2) from wild-type cDNA obtained via reverse transcription of flower bud RNA with a Retroscript Kit (Ambion, Austin, TX). The *UBQ5* cDNA fragment used to demonstrate equal loading was amplified from flower bud cDNA with primers NUBQ5 and CUBQ (Table S2). For Northern blot analysis, RNA was extracted from flower buds (all stages) with Trizol (Invitrogen, Carlsbad, CA) according to manufacturer's specifications. mRNA was isolated with PolyATtract mRNA isolation system (Promega, Madison, WI). 2  $\mu$ g of mRNA was loaded in each lane. Probes were labeled with  $^{32}$ P-dCTP with a Prime-It Kit (Stratagene, Carlsbad, CA) and used for Northern blotting as described previously [1].  
 (D) RT-PCR analysis of *POK2* gene expression in wild-type (Columbia), *pok2-1* and *pok2-2* mutant backgrounds (N, no DNA negative control; G, wild-type genomic DNA positive control). PCR was performed with 1  $\mu$ l of undiluted cDNA (und.) and 1  $\mu$ l of 1:10 diluted cDNA (1:10) as templates. Primer pairs were chosen to flank T-DNA insertion sites in each *pok2* allele (see Table S2) amplifying PCR fragments *a* (for *pok2-2* analysis) and *b* (for *pok2-1* analysis), whose locations are illustrated in (B). As a control, a fragment of the *UBQ5* gene was amplified from each template with NUBQ5 and CUBQ5 primers (Table S2). For cDNA production, 2  $\mu$ g of total RNA from 6 day-old seedlings (isolated as described earlier) was treated with DNase (Invitrogen) and reverse transcribed as described earlier.

[embnet.org/software/coils/COILS\\_doc.html](http://embnet.org/software/coils/COILS_doc.html)) throughout the entire C terminus and putative cargo binding tail domains.

We investigated the expression pattern of *POK1* and *POK2* in transgenic plants expressing a  $\beta$ -glucuronidase (GUS) reporter gene under the control of *POK1* and *POK2* putative native promoter regions. For *POK1* expression analysis, two different constructs were

analyzed that gave identical expression patterns, one with 2610 bp (*pPOK1*:GUS) and the other with 1134 bp (*mpPOK1*:GUS) upstream of the ATG. *POK2* expression was analyzed with a GUS fusion construct containing 2578 bp of upstream sequence. A variety of tissues were analyzed for GUS expression in multiple transgenic lines for all three constructs. Similar GUS expression patterns were found for both *POK1* and *POK2*, which

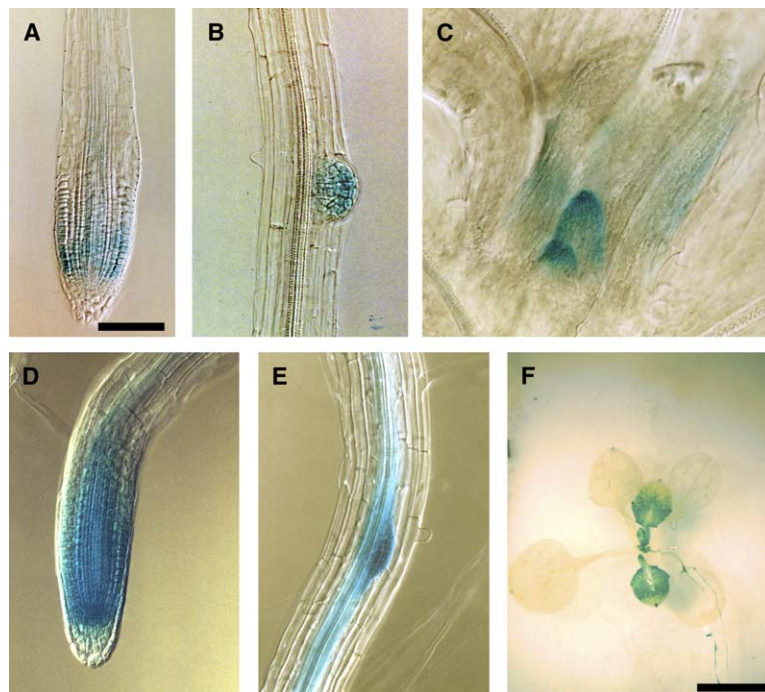
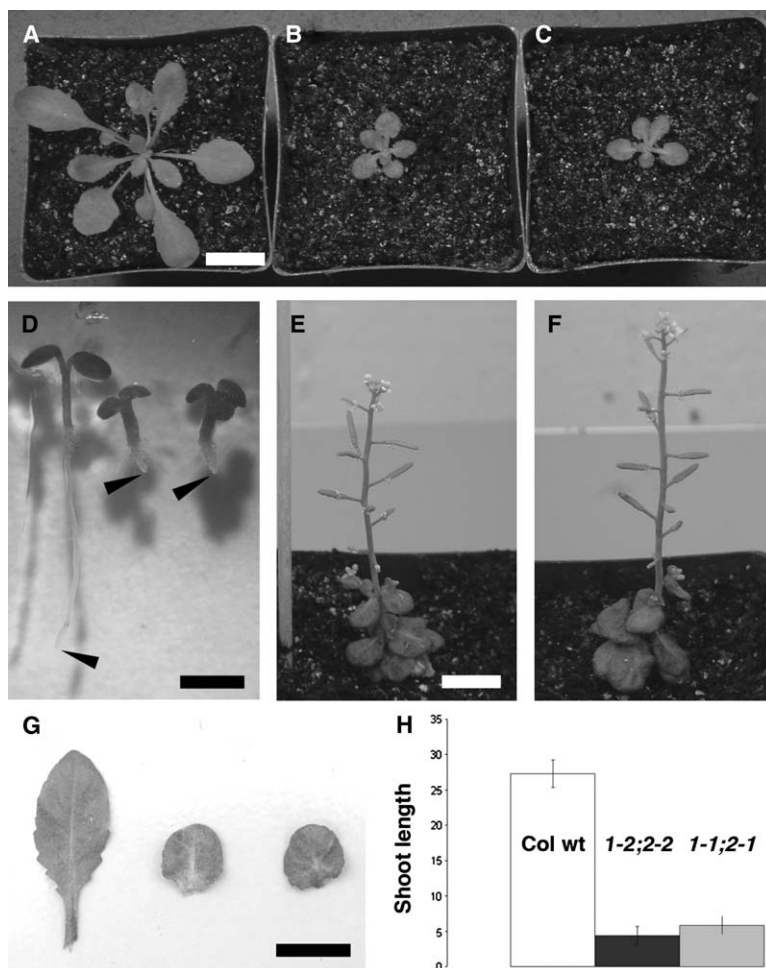


Figure 2. Gene Expression Patterns Observed in *POK* Promoter:GUS Fusion Lines  
 Regions upstream of the translation start sites specified in the text were cloned in-frame with GUS in pDW137 [22] (see Table S3 for primers).  
 (A–C) GUS reporter gene expression in *mpPOK1*:GUS lines exhibiting expression in the root apical meristem (A), lateral root meristem (B), and shoot apex (C).  
 (D–F) GUS expression in *pPOK2*:GUS lines exhibiting expression in root apical meristem (D), lateral root meristem, and root vascular tissue (E) and developing leaves of a 14-day-old seedling (F). Histochemical GUS staining was carried out as described elsewhere [23]. Scale bar equals 100  $\mu$ m (A–E) and 1 cm (F).



**Figure 3. Phenotype of *pok1;pok2* Double Mutant Plants**

(A–C) 3-week-old plants: (A) wild-type (Columbia), (B) *pok1-2;pok2-2*, (C) *pok1-1;pok2-1*. (D) Comparison of 5-day-old seedlings: left, wild-type (Columbia); middle, *pok1-2;pok2-2*; right, *pok1-1;pok2-1*. Arrowheads point to root tips. (E and F) Adult double mutant plants: *pok1-2;pok2-2* (E) and *pok1-1;pok2-1* (F). (G) Comparison of expanded leaves: left, wild-type (Columbia); middle, *pok1-2;pok2-2*; right, *pok1-1;pok2-1*. (H) Graphic representation of shoot lengths of 45-day-old plants of the indicated genotypes. Values plotted represent means of 15 plants ± SD (wild-type, 27.31 ± 1.96 cm; *pok1-2;pok2-2*, 4.40 ± 1.30 cm; *pok1-1;pok2-1*, 5.84 ± 1.33 cm). Scale bar equals 1 cm (A–C, E–G) and 0.5 cm (D).

are expressed in tissues enriched in dividing cells, such as root meristems (Figures 2A and 2D), root primordia (Figures 2B and 2E), and leaf primordia/young leaves (Figures 2C and 2F). Although the expression domains for *POK1* constructs were more limited than those for *POK2*, the intensity of GUS staining in *pPOK1:GUS* and *mpPOK1:GUS* lines was much weaker overall than in *pPOK2:GUS* lines (requiring extended incubation times to see even weak signals, unlike *pPOK2:GUS* lines, where strong staining was observed after just 2 hr of incubation with substrate). Thus, the full extent of endogenous *POK1* gene expression may not be revealed by the *pPOK1:GUS* and *mpPOK1:GUS* lines. Together with the sequence similarity between *POK1* and *POK2*, the similar GUS staining patterns observed in *POK1* and *POK2* promoter-GUS lines suggested that these genes might act redundantly. The expression domains of *POK1* and *POK2* revealed by this analysis also overlap with that of *ATN* (K. Walker and L.G.S., unpublished data), supporting the possibility of a direct interaction between *POK1/2* and *ATN* in vivo.

In order to gain insight into the function of *POK1* and *POK2*, we searched the SALK T-DNA collection database [15] (<http://signal.salk.edu/cgi-bin/tdnaexpress>) and identified T-DNA insertions in both genes. SALK\_001081 (*pok1-1*), SALK\_067862 (*pok1-2*), SALK\_013944 (*pok2-1*), and SALK\_066406 (*pok2-2*)

were obtained from the *Arabidopsis* Biological Resource Center (ABRC, Columbus, OH; all mutations are in the Columbia background). The presence of T-DNA insertions in exons was confirmed by sequencing (Figures 1A and 1B). Genotypes were analyzed with a PCR-based method (see Supplemental Data for primers). Transcript accumulation in flower bud tissues or 6-day-old seedlings, respectively, was analyzed in plants homozygous for each of the four insertions. Northern blot analysis with a *POK1* probe revealed a 6.2 kb transcript in wild-type tissues, which is consistent with the intron/exon structure of this gene. No *POK1* transcript was detected in *pok1-1* or *pok1-2* mutants (Figure 1C). Moreover, RT-PCR analysis revealed no detectable *POK2* transcripts in *pok2-1* or *pok2-2* mutants spanning their respective T-DNA insertion sites (Figure 1D).

Plants homozygous for any one of these mutant alleles did not show obvious phenotypes. Considering the similarity in both sequence and expression pattern for *POK1* and *POK2*, we generated the double mutant to uncover potentially redundant functions for these genes. *POK1* and *POK2* are closely linked on chromosome III (approximately 0.6 MB apart). *pok1-1* was crossed to *pok2-1* and *pok1-2* was crossed to *pok2-2* to create two different double heterozygotes, and F1 progeny from both crosses were backcrossed to

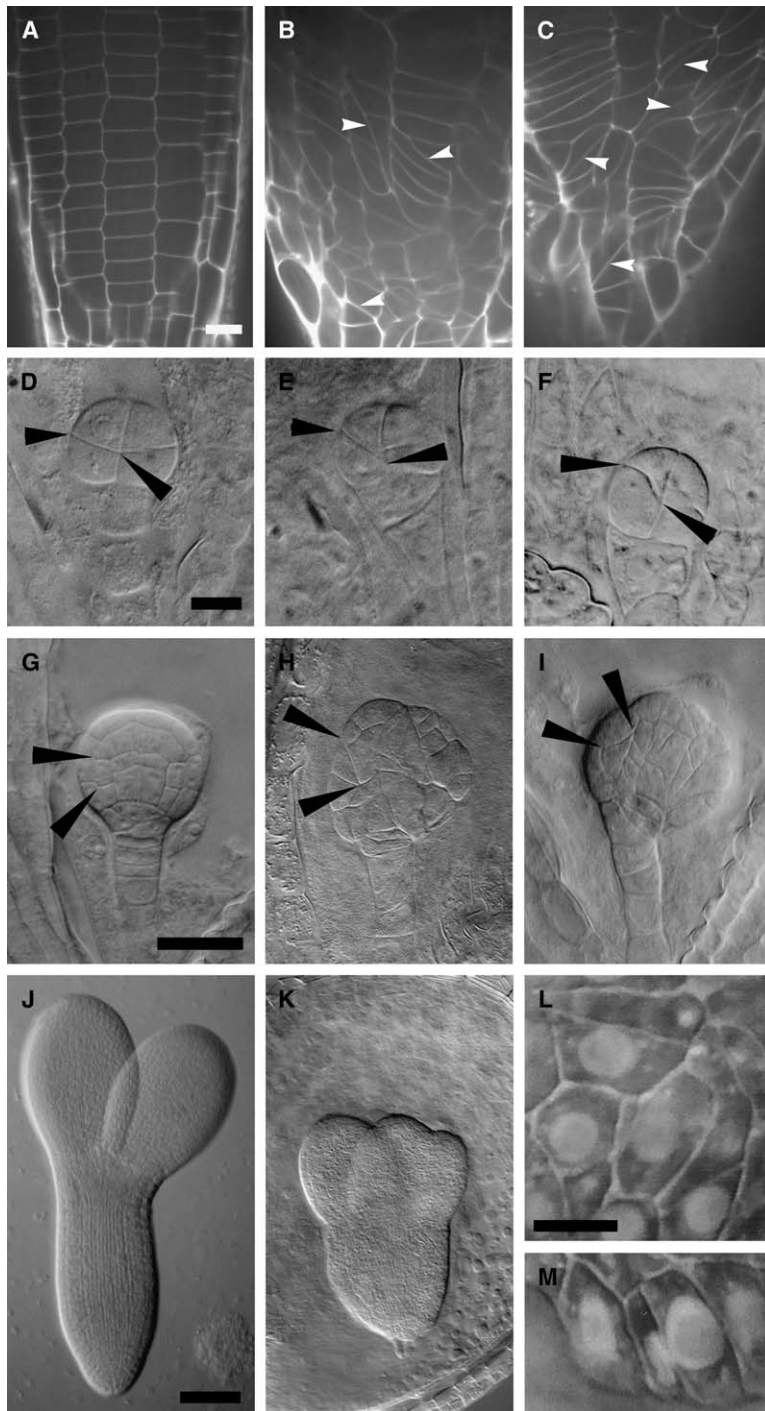


**Figure 4. Cell Wall Misorientation in *pok* Double Mutant Seedlings and Embryos**

(A–C) Propidium iodide-stained root meristems: (A) wild-type (Columbia), (B) *pok1-2; pok2-2*, (C) *pok1-1; pok2-1*. Arrowheads point to examples of misoriented cell walls. Fluorescent samples were illuminated with a 488 nm line from an argon laser and visualized with a Nikon TE-200U microscope equipped with a 100× 1.4 NA water immersion objective. Images were acquired with a Yokogawa Nipkow spinning disc confocal head, a Chroma HQ610/75 band pass emission filter, and a Coolsnap HQ cooled CCD camera controlled by MetaMorph software (Universal Imaging Corporation, Downing, PA).

(D–K) Cleared embryos viewed with DIC optics: (D–F) octant stage embryos, (G–I) globular stage embryos, (J and K) mature embryos; (D, G, J) wild-type (Columbia), (E, H, K) *pok1-2; pok2-2*, (F, I) *pok1-1; pok2-1*. Arrowheads mark boundaries of cell walls. Siliques at various stages after fertilization were fixed in methanol/acetic acid (3:1). Embryos were dissected out and cleared in chloralhydrate/water (5 g/2 ml) visualized with DIC optics with a Nikon E600 microscope. Images were captured with NIH ImageJ version 1.32j software with a DAGE MTI CCD72 camera coupled to a Scion LG-3 frame grabber.

(L and M) Random cell wall positions observed in *pok1-1; pok2-1* 3 μm sections of globular embryos. Embryos were fixed, embedded in methacrylate resin, and sectioned as described previously [24]. Images were acquired as described above. Scale bars equal 10 μm (A–D); 25 μm (G–I); 50 μm (J and K); 10 μm (L and M).

Columbia wild-type plants. 1/106 F2 plants genotyped for the *pok1-1; pok2-1* allele combination and 1/157 genotyped for the *pok1-2; pok2-2* combination contained a recombinant chromosome carrying both mutations. These double heterozygous plants were allowed to self-fertilize, and progeny were genotyped. For both allele combinations, double homozygotes showed similar defects at a variety of developmental stages, while double heterozygotes were indistinguishable from wild-type plants, indicating that the mutations are recessive. Due to linkage of *pok1* and *pok2*, the *pok1; pok2* double

mutations segregated as a single locus with approximately 1 out of 4 plants homozygous for both mutations (e.g., 38 homozygous *pok1-1; pok2-1* individuals, n = 173).

*pok1; pok2* double mutant seedlings differ from wild-type in having smaller cotyledons as well as shorter, wider roots and hypocotyls (Figures 3A–3D and Figures S3A–S3C). Adult plants exhibit a dwarfed stature, but all organs are present, although miniaturized (Figures 3E–3G, Figures S3D–S3F). Plants are fertile but produce reduced numbers of seeds. To investigate the double

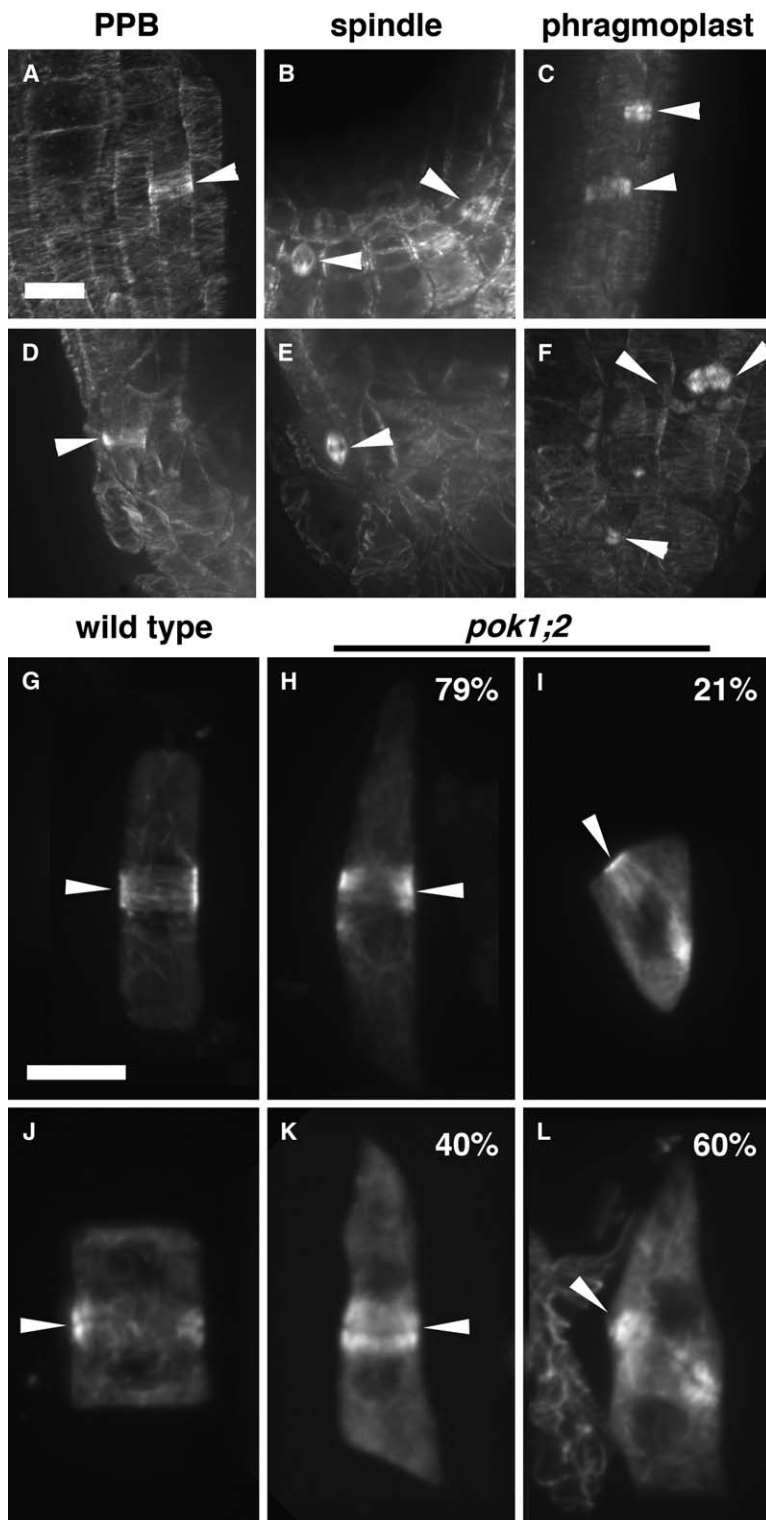


Figure 5. Visualization of Mitotic Microtubule Arrays in Root Tips via Fixation and Immunolabeling of Tubulin

(A–F) Whole mounts, arrowheads indicating mitotic microtubule arrays.

(G–L) Root tip squashes, arrowheads indicate preprophase bands (G–I) and phragmoplasts (J and K).

(A–C, G, J) Wild-type (Columbia); (D–F, H, I, K, L) *pok1-1; pok2-1*. Root squashes reveal tilted orientations of mitotic microtubule arrays in *pok1-1; pok2-1* double mutants. Whole-mount immunolabeling was carried out according to [25]. For root squashes, the same protocol was modified as follows. After the postfixation  $\text{NaBH}_4$  treatment, seedlings were digested in 1% Cellulysin (Calbiochem) for 10 to 20 min, and root tips were gently squashed onto cover slips and dried overnight. Preparations were then dehydrated in methanol and rehydrated in PBS as for whole mounts. Tubulin was labeled with anti-tubulin monoclonal antibody B512 (Sigma, St. Louis, MO) followed by FITC-conjugated anti-mouse Ig (Invitrogen). Fluorescent samples were imaged as described earlier (Figure 4 legend) except that a Chroma HQ525/50 band pass emission filter was used. Scale bars equal 10  $\mu\text{m}$ .

mutant phenotype on a cellular level, living root meristems were stained with propidium iodide (10  $\mu\text{g}/\text{ml}$  in  $\text{H}_2\text{O}$ ), which outlines cell walls in living tissues. In wild-type root meristems, cells divide transversely and longitudinally to generate a very regular cell pattern (Figure 4A). In contrast, double mutant root meristems exhibited highly disordered cell patterns with most walls lacking parallel or perpendicular alignment to the

longitudinal axis of the root and most cells exhibiting irregular shapes (Figures 4B and 4C). Examination of cell wall patterns suggested that misoriented cell divisions were largely responsible for the irregular cell pattern (e.g., arrowheads, Figures 4B and 4C). We assessed how early the mutation affects the double mutant's development. In wild-type embryos, cell divisions follow an invariant pattern [16] (e.g., Figure 4D for octant stage

embryos). In *pok1;pok2* double mutants, misplaced cell walls were observed as early as the octant stage of embryogenesis (Figures 4E and 4F). Throughout embryogenesis, the mispositioning of cell walls continues (see double mutants, Figures 4H and 4I, versus wild-type, Figure 4G), eventually giving rise to slightly misshapen mature embryos with a stubby appearance (Figure 4K) compared to wild-type (Figure 4J). Incomplete cell walls and wall stubs, a common feature of cytokinesis-defective mutants [17–19], were not observed in Toluidine blue-stained sections of double mutant embryos (Figures 4L and 4M), nor in propidium iodide-stained root meristems (Figures 4B and 4C). These results suggest that *POK1* and *POK2* are not involved in the formation or maturation of the cell wall but are required for its correct positioning.

To investigate the basis of cell wall placement defects in *pok1;pok2* double mutants, we immunolabeled microtubules to visualize mitotic microtubule arrays. Whole-mount staining of root meristems revealed that all mitotic arrays were present in double mutants (Figures 5D–5F) as in wild-type (Figures 5A–5C). Although both straight and curved phragmoplasts could be observed in these whole mounts, the orientations of most mitotic arrays was obscure due to irregular cell shapes and orientations. To overcome this limitation, root squashes were prepared for immunolocalization of microtubules (Figures 5G–5L). In *pok1-1;pok2-1* roots, 79% of PPBs were perpendicular to the longitudinal cell axis (Figure 5H), while 21% were tilted (neither parallel nor perpendicular to the long axis, Figure 5I,  $n = 34$ ); only 4% of wild-type PPBs were tilted ( $n = 44$ , Figure 5G). All wild-type phragmoplasts analyzed ( $n = 26$ ) were positioned parallel or perpendicular to the longitudinal cell axis (Figure 5J). In *pok1-1;pok2-1* double mutants, 60% of the phragmoplasts analyzed ( $n = 32$ ) were tilted from the expected position (e.g., Figure 5L), while 40% were transverse or parallel to the longitudinal cell axis (e.g., Figure 5K). Since the frequency of transverse phragmoplasts in *pok1-1;pok2-1* double mutant cells (40%) is greatly reduced compared to that of transverse PPBs (79%), these results indicate that, as in maize *tan1* mutants, misplacement of cell walls in *pok1;pok2* double mutants can be attributed largely to a failure of phragmoplast guidance to the site previously occupied by the PPB.

In this study, we identified two previously unstudied kinesins in *A. thaliana*, *POK1* and *POK2*, and showed that they are functionally redundant proteins involved in the spatial control of cytokinesis. The mechanisms leading to properly oriented cell division in plants are poorly understood, and there are many possible roles for kinesins in this process. Proper orientation of cell division planes involves an interaction between the expanding phragmoplast and the cortical division site, an interaction that appears to be defective in *pok1;pok2* double mutants. A dynamic population of endoplasmic microtubules links the dividing nucleus to the cell cortex throughout mitosis and cytokinesis [20, 21], suggesting the possibility that *POK1/2* could mediate microtubule-dependent interactions between the dividing nucleus and the cortex that are important for phragmoplast guidance. Maize homologs of *POK1* and *POK2* were initially identified as potential binding partners of *TAN1* in a yeast

two-hybrid screen, and the COOH terminus of *POK1* (containing the putative cargo binding domain) interacts with the *A. thaliana* homolog of *TAN1*, *ATN*. Combined with our finding that the *pok1;pok2* double mutant phenotype in *A. thaliana* closely resembles the *tan1* mutant phenotype in maize, these findings suggest that *POK1* and *POK2* directly interact with *ATN* to achieve their functions in cytokinesis. One hypothesis is that *POK1/2* transports *ATN* to its site(s) of action, moving *ATN* along microtubules within mitotic arrays or along endoplasmic microtubules linking the dividing nucleus to the cell cortex. Further work will be required to elucidate the roles of *POK1* and *POK2* in the spatial control of cytokinesis and their relationship to *ATN*.

#### Supplemental Data

Supplemental Data include three figures and three tables and can be found with this article online at <http://www.current-biology.com/cgi/content/full/16/9/888/DC1/>.

#### Acknowledgments

We thank Amanda Overton and Andreas Chandra for help with genotyping. We are also grateful to former and present members of the Smith lab for stimulating discussions. T-DNA insertion lines were obtained from the ABRC. This work was supported by NIH grant GM53137 to L.G.S. and a fellowship from the Austrian Science Fund to S.M. (project J2241-B04).

Received: February 13, 2006

Revised: March 2, 2006

Accepted: March 3, 2006

Published: May 8, 2006

#### References

1. Smith, L.G., Gerttula, S.M., Han, S., and Levy, J. (2001). TANGLED1: a microtubule binding protein required for the spatial control of cytokinesis in maize. *J. Cell Biol.* 152, 231–236.
2. Cleary, A.L., and Smith, L.G. (1998). The *Tangled1* gene is required for spatial control of cytoskeletal arrays associated with cell division during maize leaf development. *Plant Cell* 10, 1875–1888.
3. Smith, L.G., Hake, S., and Sylvester, A.W. (1996). The *tangled1* mutation alters cell division orientations throughout maize leaf development without altering leaf shape. *Development* 122, 481–489.
4. Smith, L.G. (2001). Plant cell division: building walls in the right places. *Nat. Rev. Mol. Cell Biol.* 2, 33–39.
5. Vanstraelen, M., Van Damme, D., De Rycke, R., Mylle, E., Inze, D., and Geelen, D. (2006). Cell cycle-dependent targeting of a kinesin at the plasma membrane demarcates the division site in plant cells. *Curr. Biol.* 16, 308–314.
6. Otegui, M., and Staehelin, L.A. (2000). Cytokinesis in flowering plants: more than one way to divide a cell. *Curr. Opin. Plant Biol.* 3, 493–502.
7. Mineyuki, Y., and Palevitz, B.A. (1990). Relationship between preprophase band organization, F-actin and the division site in *Allium*. *J. Cell Sci.* 97, 527–537.
8. Wick, S.M. (1991). Spatial aspects of cytokinesis in plant cells. *Curr. Opin. Cell Biol.* 3, 253–260.
9. Molchan, T.M., Valster, A.H., and Hepler, P.K. (2002). Actomyosin promotes cell plate alignment and late lateral expansion in *Tradescantia* stamen hair cells. *Planta* 214, 683–693.
10. Holweg, C., and Nick, P. (2004). *Arabidopsis* myosin XI mutant is defective in organelle movement and polar auxin transport. *Proc. Natl. Acad. Sci. USA* 101, 10488–10493.
11. Reddy, A.S., and Day, I.S. (2001). Kinesins in the *Arabidopsis* genome: a comparative analysis among eukaryotes. *BMC Genomics* 2, 2.
12. Schliwa, M., and Woehlke, G. (2003). Molecular motors. *Nature* 422, 759–765.

13. Lawrence, C.J., Dawe, R.K., Christie, K.R., Cleveland, D.W., Dawson, S.C., Endow, S.A., Goldstein, L.S., Goodson, H.V., Hirakawa, N., Howard, J., et al. (2004). A standardized kinesin nomenclature. *J. Cell Biol.* **167**, 19–22.
14. Pan, R., Lee, Y.R., and Liu, B. (2004). Localization of two homologous *Arabidopsis* kinesin-related proteins in the phragmoplast. *Planta* **220**, 156–164.
15. Alonso, J.M., Stepanova, A.N., Leisse, T.J., Kim, C.J., Chen, H., Shinn, P., Stevenson, D.K., Zimmerman, J., Barajas, P., Cheuk, R., et al. (2003). Genome-wide insertional mutagenesis of *Arabidopsis thaliana*. *Science* **301**, 653–657.
16. Westhoff, P., Jesker, H., Jurgens, G., Klopstech, K., and Link, G. (1996). Embryogenese. In *Molekulare Entwicklungsbiologie: Vom Gen zur Pflanze* (New York: Georg Thieme Verlag Stuttgart), pp. 117–126.
17. Jurgens, G. (2005). Cytokinesis in higher plants. *Annu. Rev. Plant Biol.* **56**, 281–299.
18. Waizenegger, I., Lukowitz, W., Assaad, F., Schwarz, H., Jurgens, G., and Mayer, U. (2000). The *Arabidopsis* KNOLLE and KEULE genes interact to promote vesicle fusion during cytokinesis. *Curr. Biol.* **10**, 1371–1374.
19. Muller, S., Fuchs, E., Ovecka, M., Wysocka-Diller, J., Benfey, P.N., and Hauser, M.-T. (2002). Two new loci, *PLEIADE* and *HYADE*, implicate organ-specific regulation of cytokinesis in *Arabidopsis*. *Plant Physiol.* **130**, 312–324.
20. Dhonukshe, P., Mathur, J., Hulskamp, M., and Gadella, T.W.J. (2005). Microtubule plus-ends reveal essential links between intracellular polarization and localized modulation of endocytosis during division-plane establishment in plant cells. *BMC Biol.* **3**, 11.
21. Wick, S.M. (1985). Immunofluorescence microscopy of tubulin and microtubule arrays in plant cells. III. Transition between mitotic/cytokinetic and interphase microtubule arrays. *Cell Biol. Int. Rep.* **9**, 357–371.
22. Blazquez, M.A., Soowal, L.N., Lee, I., and Weigel, D. (1997). *LEAFY* expression and flower initiation in *Arabidopsis*. *Development* **124**, 3835–3844.
23. Hauser, M.-T., and Bauer, E. (2000). Histochemical analysis of root meristem activity in *Arabidopsis thaliana* using a cyclin:GUS ( $\beta$ -glucuronidase) marker line. *Plant Soil* **226**, 1–10.
24. Frank, M.J., Cartwright, H.N., and Smith, L.G. (2003). Three Brick genes have distinct function in a common pathway promoting polarized cell division and cell morphogenesis in maize leaf epidermis. *Development* **130**, 753–762.
25. Sugimoto, K., Williamson, R.E., and Wasteneys, G.O. (2000). New techniques enable comparative analysis of microtubule orientation, wall texture, and growth rate in intact roots of *Arabidopsis*. *Plant Physiol.* **124**, 1493–1506.

#### Accession Numbers

The GenBank accession numbers for full-length cDNA sequences are DQ399529 (*POK1*) and DQ399530 (*POK2*).